Comparative Analysis of Data Acquisition Setups for Fast Timing in ToF-PET Applications

Riccardo Latella, Antonio J. Gonzalez, *Member, IEEE*, José M. Benlloch, Paul Lecoq, *Fellow, IEEE*, and Georgios Konstantinou, *Member, IEEE*

***Abstract*—The signal-to-noise ratio in positron emission tomography (PET) improves with precise timing resolution. PET systems enabling the capability of time-of-flight (ToF) are nowadays available. This study assesses various data configurations, comparing the obtained timing performances applicable to time-of-flight positron emission tomography (ToF-PET) systems. Different readout configurations were evaluated together with silicon photomultipliers (SiPMs) photosensors from the Fondazione Bruno Kessler (FBK), with and without the so-called metal trench (MT) technology. The tests were carried out with scintillation crystals of 3×3×5 mm^3 (LYSO:Ce,Ca) from SIPAT. Two onboard FPGA-based systems, namely, the Felix time-to-digital converter (TDC) from Tediel S.r.l. and the ASIC-based FastIC from the University of Barcelona, along with custom-made high-frequency electronics (CM-HF), were compared. Considering only photopeak events, the best-coincidence timing resolution (CTR) results obtained were 71 ps with the MT SiPMs. This result worsened to 88 ps with the old version of the same device that does not include the MT technology (called HD). The results demonstrate substantial CTR improvements when MT SiPMs were used across the different scenarios, resulting in a timing improvement in the 10 to 45-ps range compared to HD SiPMs. Notably, the Felix TDC achieved sub-100-ps timing results, emphasizing the potential of FPGA technology in ToF-PET applications. Moreover, the fully passive version of the CM-HF connected to the MT SiPMs shows only a degradation of 8-ps difference compared to the version using amplifiers. The novel MT-type SiPMs promise superior timing performance, enhancing accuracy and efficiency in PET imaging systems.**

***Index Terms*—DAQ, lutetium yttrium oxyorthosilicate (LYSO), metal trenches, NUV, time-of-flight positron emission tomography (ToF-PET).**

I. Introduction

TIME-OF-FLIGHT positron emission tomography (ToF-PET) is an important medical imaging technique used for visualizing organs and tissues as well as their functionality. positron emission tomography (PET) is crucial in diagnosing and monitoring various diseases, including cancer, cardiovascular conditions, as well as neurological disorders [1], [2].

A key component of ToF-PET scanners is the scintillation detector, which detects annihilation's photons produced after the administration of a positron emitter radio-pharmaceutical to the patient. These detectors employ scintillation materials to convert these photons into low-energy scintillation light. Originally, thallium-doped sodium iodide (NaI:Tl) and bismuth germanate (BGO) crystals were widely used. However, they were replaced by lutetium-based scintillators, such as lutetium oxyorthosilicate (LSO) and lutetium yttrium oxyorthosilicate (LYSO), since those offer advantages, such as higher-light yield, fast scintillation decay time, and good detection efficiency [3], [4].

In particular, LYSO doped with cerium (LYSO:Ce) has been positioned as the leading scintillator material for ToF-PET detectors. It offers a high-light yield of up to 40 000 photons per MeV and a 7.2 g/cm^3 density, making it highly sensitive to radiation detection. Additionally, LYSO exhibits a fast scintillation decay time of around 30–40 ns, enabling accurate timing determination [5], [6]. A step further has been taken by co-doping these crystals with calcium (LYSO:Ce,Ca), leading to better-decay times and, so, coincidence time resolution (CTR) values [7].

In terms of photodetectors, silicon photomultipliers (SiPMs) have gained popularity in ToF-PET detectors due to their compact design, low cost, and fast response to incident light [8], [9], [10]. SiPMs consist of arrays of single-photon avalanche diodes (SPADs) and offer advantages, such as insensitivity to magnetic fields, high-quantum efficiency, and a smaller form factor, compared to traditional photomultiplier tubes (PMTs). SiPMs preserve the ToF information crucial for accurate timing measurements and have contributed to advancements in ToF-PET imaging [11], [12], [13].

The choice of scintillation material and photo-detector technology in ToF-PET systems is critical for achieving optimal image quality. While LYSO-based detectors offer superior timing resolution and good detection efficiency performance, other factors, such as cost, size, and compatibility with other imaging modalities (like computed tomography and magnetic resonance imaging), must also be considered. Ongoing research and development efforts focus on further improving the performance of ToF-PET detectors, including

Manuscript received 21 March 2024; revised 9 May 2024; accepted 12 May 2024. Date of publication 15 May 2024; date of current version 5 September 2024. This work was supported in part by the frame of the ERC Advanced Grant TICAL under Grant 338953 PI (P. Lecoq), and the related Prof-of-Concept Project ULTIMA under Grant 680552, both funded by the European Commission; and in part by the European Research Council (ERC) through the European Union's Horizon 2020 Research and Innovation Program under Grant 695536. *(Corresponding author: Riccardo Latella.)*

This work did not involve human subjects or animals in its research.

Riccardo Latella, Paul Lecoq, and Georgios Konstantinou are with Multiwave Metacrystal S.A., Geneva, Switzerland, and also with Institue for Instrumentation in Molecular Imaging, 46011 Valencia, Spain (e-mail: rlatell@upv.es).

Antonio J. Gonzalez and José M. Benlloch are with the Department of Detectors, Institue for Instrumentation in Molecular Imaging, 46011 Valencia, Spain.

Color versions of one or more figures in this article are available at https://doi.org/10.1109/TRPMS.2024.3401391.

Digital Object Identifier 10.1109/TRPMS.2024.3401391

advancements in scintillator materials, photo-detectors, and readout electronics [14], [15], [16].

Moreover, the choice of readout technology in ToF-PET systems plays a vital role in time and spatial resolution. Scintillators and photodetectors have been significantly investigated to achieve the desired spatial and CTR goals. However, a scalable readout system that can reach 10-ps FWHM CTR performance, leading to a ToF spatial resolution of 1.5 mm, remains a challenge, especially keeping a useful physical sensitivity [17]. Achieving optimal timing information in readout systems typically requires significant power consumption for signal amplification, resulting in large electronics volumes, excessive cooling, and cost at the scanner system level.

This study contributes to the discussion as a collection of different aspects in the context of basic research to improve timing performance for single line-of-response (LOR) testbenches. Indeed, we introduce the use of novel broadband amplifiers beyond silicon for SiPM readout. Additionally, it compares simulation and experimental data from various scalable technologies, focusing on their timing performance, using LYSO:Ce,Ca scintillators. Finally, we evaluate a ToF scenario by introducing a double-source radioactive phantom (DSRP) designed for a single LOR, demonstrating the resolution capabilities and linearity of the two activities through ToF [18]. By analyzing various scenarios, including the choice of photodetectors and readout systems, the study seeks to guide future improvements in the resolution and image quality of ToF-PET scanners.

II. Materials and Methods

A. Front-End Characteristics

We employed LYSO:Ce,Ca crystals for their fast-timing response and stopping power. The crystal samples have dimensions of $3\times3\times5$ mm^3 with all surfaces polished and covered with ESR films (wrapped with Teflon thereafter) except for the extraction face. This double coating has been proven very effective in reducing light escaping from the corners of the crystals. Additionally, the Teflon degradation caused by the contact with the optical grease does not impact the timing performance when reapplying the optical grease [19].

Two SiPMs, based on the same technology, are compared in coincidence experiments. These devices have no protective layer on top of the silicon, making them very fragile; however, prior testing has demonstrated the superiority of CTR by such bare devices [20]. A small quantity of epoxy resin has been placed on the bonding wires to improve their robustness. Starting from the near-ultraviolet high-field (NUV-HD, named HD) technology, Fondazione Bruno Kessler (FBK) and Broadcom jointly developed the metal trenches (NUV-HD-MT, called MT) technology, adding metal-filled deep trench isolation to suppress cross-talk, allowing for significantly higher-bias voltages [21].

Finally, we use silicon solutions (SS-988) optical grease to couple the crystals to the SiPMs. For reference in the rest of the text, we consider the entire front-end structure as gamma sensors, composed of scintillating crystal, coupling material, and SiPM. Details of the data acquisition devices used in this work can be found in Table I.

TABLE I
Data Acquisition Devices

Name	Manufacturer	Assigned Name
Custom-Made High-Frequency (CM-HF) Boards	Metacrystal S.A.	CM-HF
FastIC Evaluation Board	CERN and University of Barcelona	FastIC
Felix Time-To-Digital (TDC)	Tediel S.r.l.	Felix
RTP084 Oscilloscope	Rohde & Schwarz	RTP

A black foam box filled with silica bags protects the coincidence setup from ambient light and humidity. Small holes have been made to introduce the supply cables, the oscilloscope probes, the temperature sensor, and the compressed air for temperature stabilization (range of 25 °C–26 °C with variations below ±0.5 °C).

The signals are selected in a coincidence window of ±1 ns and filtered (through an energy/voltage filter) to only use those in the photopeak region of the energy spectrum, using as a reference point the valley between Compton edge and photoelectric regions corresponding to an energy range of around 350–650 keV.

All the acquisitions made for this work are then post-processed using a custom Python extraction and analysis code to detect features, such as different CTR voltage thresholds (VthCTR) for each voltage bias (Vbias), analyzed and to sanitize the acquired events to discard the ones wrongly acquired.

B. Acquisition Chain Scenarios

To assess timing capabilities, we compared different scenarios with varying combinations of readout and data analysis tools while keeping the front-end consistent (see Fig. 1). An exception was made for the custom-made high-frequency (CM-HF) board, which required a modification to provide positive pulses for compatibility with the Felix time-to-digital converter (TDC) input comparators, denoted as CM-HF*. This modified version bypasses all the amplifiers on the board using some "trace-jumpers," leaving on the board just passive components. As explained in [22], this purely passive board presents a weaker and slower timing signal but a DC power consumption close to zero. To compare with this modified version of the CM-HF, scenarios with an asterisk are introduced.

Table II lists the studied data acquisition chain scenarios, each identified by a number indicating the chosen data acquisition path and a letter representing the SiPM used in the test ("HD" for NUV-HD and "MT" for NUV-HD-MT). Each scenario includes the same number of coincidence events providing different acquisition times depending on the device with lower-count rate limitation in each acquisition chain.

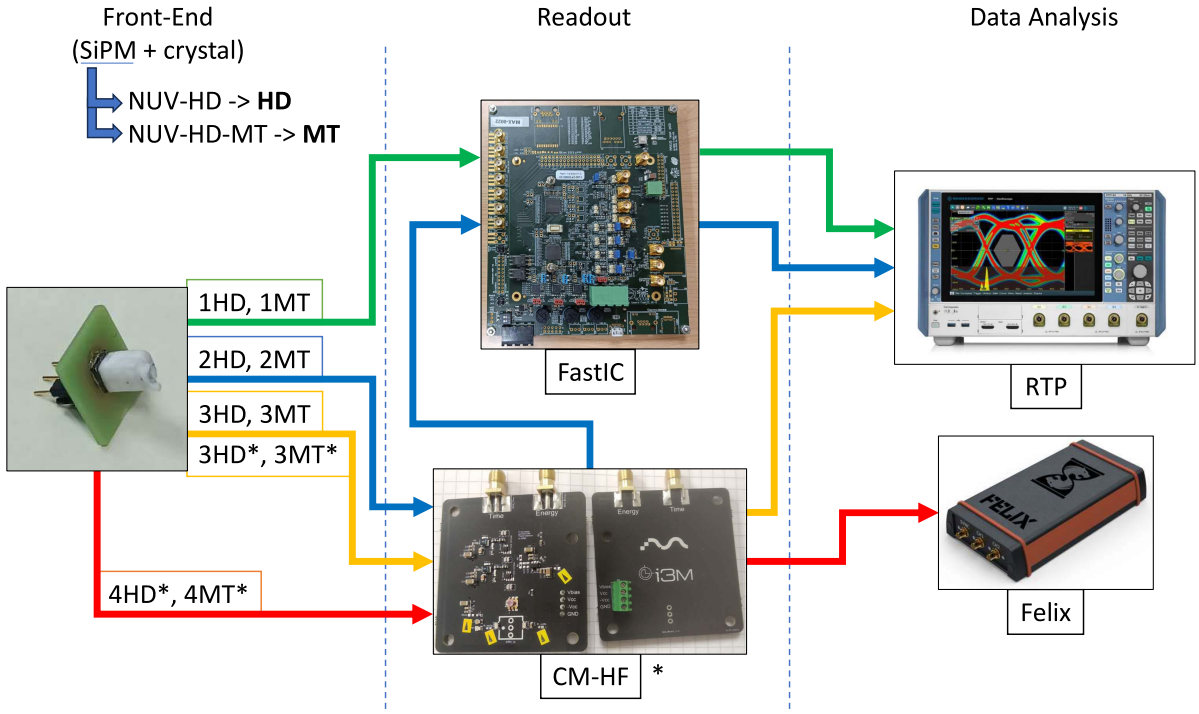

Fig. 1. Different data acquisition chain scenarios available in this work. Each scenario has been tested with both NUV-HD (case HD) and NUV-HD-MT (case MT). Scenarios marked with an asterisk indicate the utilization of the modified CM-HF version without amplifiers.

TABLE II
AVAILABLE SCENARIOS

Scenarios		Readout	Data Analysis
Name	Color		
1HD, 1MT	Green	FastIC	RTP
2HD, 2MT	Blue	CM-HF + FastIC	RTP
3HD, 3MT	Yellow	CM-HF	RTP
3HD*, 3MT*	Yellow	CM-HF*	RTP
4HD*, 4MT*	Red	CM-HF*	Felix

C. RTP084 Oscilloscope

The Rhode & Schwarz RTP084 high-performance oscilloscope was employed in scenarios where the Felix TDC was not utilized. It provides a comprehensive understanding of the pulse dynamic, facilitating the extraction of all available signal features. This oscilloscope is characterized by its rapid data acquisition capability, achieving an acquisition rate of 750 000 waveforms per second. With an 8-GHz bandwidth, four-channel configuration, 10-bit ADC resolution, ultrafast 40 Gsamples per second sampling rate, and advanced triggering options, it is a precise tool for signal analysis, enabling in-depth troubleshooting and rigorous testing across a spectrum of applications. For all measurements involving this device and a signal delivering timing information, the voltage resolution has been adjusted to get close to the noise level and, further, to improve the voltage resolution as much as possible using only 50 mV of the voltage dynamic range.

D. FastIC ASIC Demonstration Boards

This evaluation board is equipped with two 8-channel FastIC ASICs that leverage CMOS 65-nm technology with both positive and negative polarity acceptance pulse capabilities, particularly in the context of high-energy physics experiments. The board incorporates analog summation functionality for up to four channels, improving time resolution within SiPM segmentation. The ASIC provides precise Time-of-Arrival (ToA) data and linear energy measurements across a wide input peak current range, from 5 to 25 μA, with a power consumption of approximately 12-mW per channel at default settings and a maximum rate of around 50 MHz [23].

The ASIC employs current mode signal processing, generating three signal replicas upon receiving the sensor's input, enabling precise time and energy measurements. Output flexibility allows for ToA information, time over threshold (ToT) information, or a combination of both. For each of the four scenarios (1HD, 1MT, 2HD, and 2MT) involving this ASIC, distinct registry configurations have been necessary due to gain variations in the SiPMs used and the difference in the preamplifications.

The demonstration board enables SiPM inputs to be directly connected to one of the eight inputs of the two ASICs (Scenario 1). Additionally, another configuration facilitates the injection of output signals from external boards into one of the ASIC channels, potentially enhancing timing capabilities (Scenario 2). The signal is extracted through an SMA connector and subsequently subjected to coincidence analysis using an oscilloscope. The resulting output pulses are shown in Fig. 2.

E. Felix TDC

The Felix TDC [24], by Tediel S.r.l., is a low-cross-talk [25] instrument for precision engineering applications. It offers two channels (CH1 and CH2) and a SYNC input for

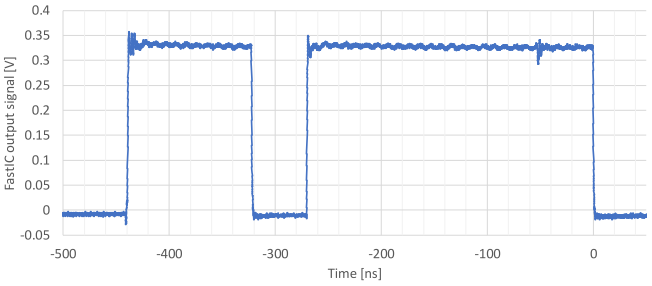

Fig. 2. Output signal of the FastIC evaluation board. The first squared wave contains the timing information, while the second contains the energy content. The length of the timing channel is arbitrary since only the rising edge contains the timing information, while the energy pulse length stores the energy information.

TABLE III
FELIX'S FEATURES AND CHARACTERISTICS

Feature	Value
Single-Shot Channel Precision	12 ps r.m.s.
Resolution (LSB)	36.6 fs
Dead–Time	25 ns
Global Measurement Rate	140 Msps
Channel Measurement Rate	80 Msps
Absolute INL	19 ps
Absolute DNL	0.8 ps
Input Voltage Level	0 V - 3.3V
Programmable Threshold Level	0V - 2.5 V

event detection and synchronization in scientific experiments. It includes customizable threshold comparators for precise adaptation to input signals. Felix handles 140 million samples per second.

Felix is based on USB-C connectors together with a framing protocol [26]. Each channel includes a dedicated indicator for real-time setup monitoring. The software, developed in C++, provides a graphical interface and command-line functionality. Felix is platform-agnostic, thus ensuring compatibility with various setups (Table III).

Measurements done with the Felix have been conducted in two steps. First, the τ distribution between two detectors ($\Delta\tau = t1 - t2$) is built using real-time, on-chip histogrammers [27] and directly monitored from the dedicated software, which allows quick detection of coincidence events. Then, all the rising and falling edge timestamps for the detected events are easily extracted for post-processing analysis.

F. CM-HF Design Simulation

This board design represents a state-of-the-art approach to timing, building upon prior works in the field [28], primarily focused on single-pixel CTR analysis. Our front-end electronic boards incorporate concepts previously published [29] and have been enhanced through specific modifications [22], [30]. Our front-end maintains the same timing capabilities compared

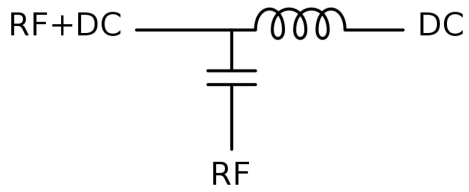

Fig. 3. Equivalent circuit of a bias tee.

to previous works but with a reduced power requirement. We designed the PCB and selected the components to fully harness the oscilloscope's broadband capability, spanning from DC to 8 GHz. It is a double-channel readout circuit with a dedicated timing channel based on a Balun (short for balanced-to-unbalanced) transformer. This passive component is primarily designed to match signals between balanced and unbalanced transmission lines [31], [32]. In our design, a 1:2 impedance ratio Balun transformer from MACOM (model: MABA-011118) with a high-broadband frequency domain (10 MHz–10 GHz) effectively steps up the voltage across the secondary side compared to the primary side, doubling the voltage across the load. While a Balun can provide voltage step-up and better-impedance matching, it does not have an active stage like transistors in amplifiers. However, when coupled with the high-precision DAQ stage of the oscilloscope, it can improve the signal-to-noise ratio passively, providing a small gain to the SiPM HF signal and enhancing the common-mode rejection ratio of the balance port [33].

The output of the Balun transformer is then fed into a gallium arsenide indium gallium phosphide heterojunction bipolar transistor (GaAs InGaP HBT) amplifier (HMC311SC70E). Based on the Darlington configuration, the architecture of such amplifier requires a dedicated Bias-T circuit to decouple DC and AC components. A Bias-T is a diplexer, a passive structure that implements frequency-domain multiplexing. It is a three-port network (Fig. 3) that sets the DC bias point in the low-frequency port, passes the radio-frequency (RF) signals in the high-frequency port while blocking the biasing levels, and, finally, connects both DC bias and RF signal in the combined RF+DC port.

Achieving wide-band coverage across a broad range of frequencies is a complex task due to the substantial influence of parasitic effects. These effects often lead to a decline in gain performance as frequency increases. A significant shortcoming is the inductor's performance, especially self-resonance. Designing a Bias-T involves damped low-pass filter sections to manage return loss and isolation across different frequencies. Key specifications include insertion loss, bandwidth, return loss, isolation, and current. Ideally, we would like to design a Bias-T with a 0-dB insertion loss and a low-return loss in the frequency domain needed by the system. In our case, the Balun transformer gives the bandwidth limitation for the lower band (10 MHz) and the timing amplifier for the higher one (8 GHz) [34], [35]. To validate the performance of the bias-T design, an LTspice test was conducted, comparing the standard bias-T implementation with a pass-band modified version.

Fig. 4 shows the overall CM-HF schematic. Particular care has been given to the routing and component placement on the

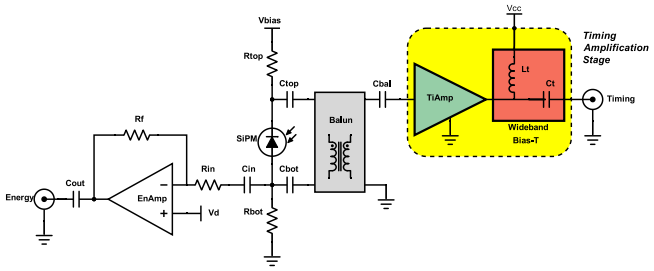

Fig. 4. Double channel CM-HF schematic.

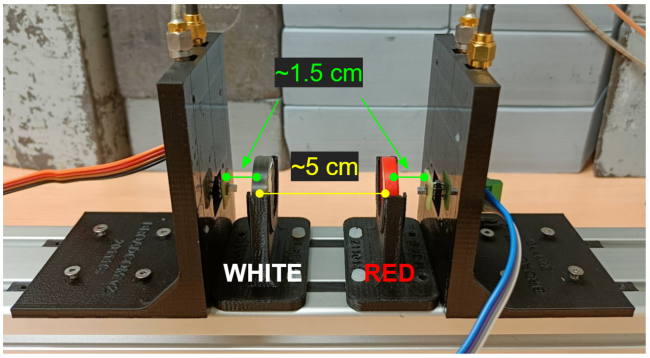

Fig. 5. DSRP with 5-cm distance between the two sources.

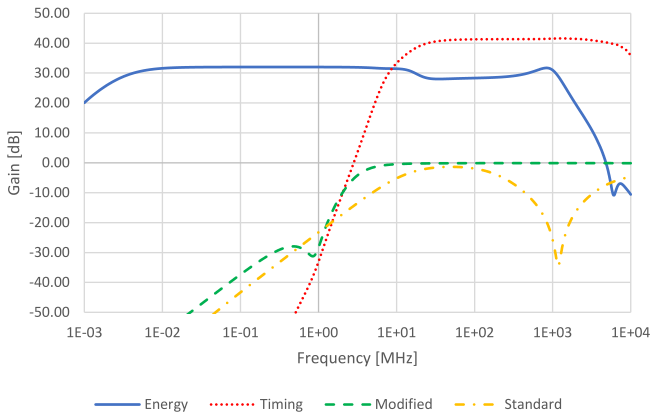

Fig. 6. Bode diagram of the simulated Bias-T and CM-HF frequency response. Solid blue and dotted red lines display the energy and timing channels of the CM-HF. Dashed-dotted yellow and dashed green lines exhibit the insertion loss of the standard and modified Bias-T versions.

PCB, aiming for 50-Ohm compatibility, minimal reflection, and minimizing current-loop induction [36], [37]. Another simulation test was carried out to assess the overall frequency performance of the timing and energy channels.

G. SiPM Characterization

A test to determine the optimal Vbias has been conducted for both SiPMs to find the best conditions in terms of CTR with the CM-HF circuit. This result has been used for the rest of the tests on the other readout and data analysis tools, given that readout electronics do not affect Vbias optimization. Simultaneously, we analyzed the optimal VthCTR for all Vbias settings.

Analysis of dark counts and cross-talk were performed to identify the threshold of the first few photons detected by the SiPM. First, the dark count rate (DCR) is measured by applying the optimal Vbias and recording the number of counts in a 1 ms period.

The DCR is the frequency of spontaneous breakdowns of a Geiger-mode SPAD triggered by thermally generated electrons, which are indistinguishable from actual photon counts [38]. Next, the cross-talk probability is evaluated from the DCR data as the ratio between the first and second event count rates. Cross-talk occurs when a secondary photon generates an electron-hole pair close to a neighboring cell, which can cause their discharge. The carriers can diffuse to the micro-cell and cause their discharge, known as “delayed optical cross-talk” [39].

To evaluate the system’s linearity [40], we utilized a DSRP, positioning two Na-22 sources at fixed distances of 3.5 and 5 cm (Fig. 5), each 1.5-cm away from the closest SiPMs and an active dimension of 0.25 mm. In contrast to previous works [32], [41] that typically employ a single source for linearity characterization, moving it across various distances, our approach allows for simultaneous comparison under different count rates, enhancing the robustness of the linearity test by directly contrasting the responses from two distinct radioactivity levels. In our case, the two sources, with activities of 407 kBq (white source) and 240.5 (red source), respectively, facilitated a comparative analysis under varied count rates. While the DSRP primarily aids in understanding the ToF reconstruction process, we mention its potential utility in exploring new scintillating materials. However, the primary focus here remains validating the SiPMs’ performance and linearity under distinct operational conditions. Future studies may further elaborate on the multitiming-kernel approach within different contexts [42].

III. Results

A. CM-HF Simulation

The simulation results of the Bias-T and CM-HF circuits are shown in the Bode diagram of Fig. 6. In particular, the standard and modified versions of the Bias-T insertion-loss are plotted in dashed-dotted yellow and dashed green lines. The energy and timing channels of the CM-HF are represented in solid blue and dotted red lines, respectively. The timing signal exhibits a plateau gain of approximately 40 dB within the 10-MHz to 10-GHz range, which is the frequency range needed by the signal frequency content of the timing channel to reach the oscilloscope unperturbed. In contrast, the energy signal has a broader region, ideally extending to DC. The wide frequency coverage achieved by this custom-made design is evident in both energy and timing outputs.

B. SiPM Characterization

For scenarios 3HD and 3MT, a Vbias analysis was conducted to compare the timing performance under different over-voltage settings. A significant improvement in timing accuracy with higher-over-voltage for the MT SiPMs is observed in Fig. 7 (see solid circles and lines). These findings

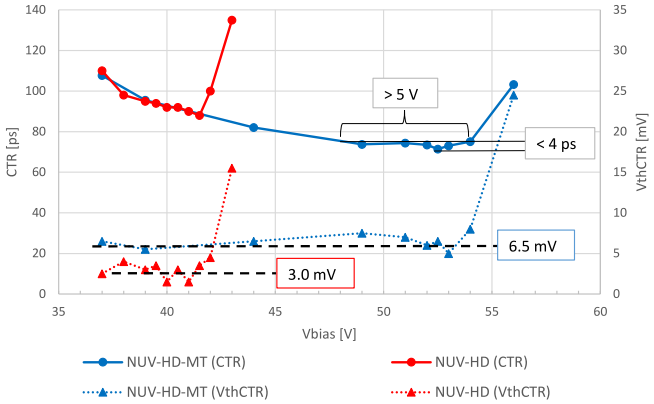

Fig. 7. Vbias scan for scenarios 3HD and 3MT considering CTR (circles) and VthCTR (triangles). A trend line has been plotted for all cases, a solid line for CTR and a dotted line for VthCTR results. A black dashed line for each SiPM highlights the average of only those VthCTR below 10 mV.

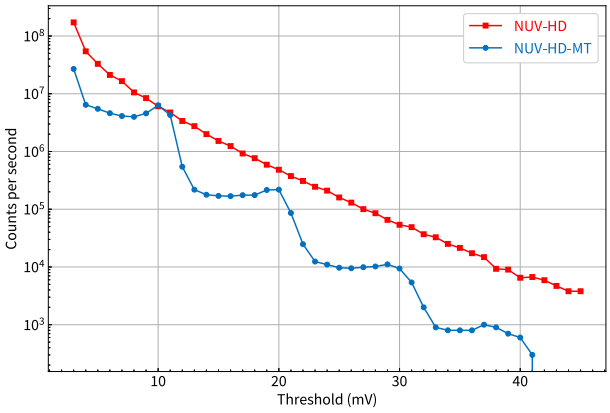

Fig. 8. DCR staircase plot showing the threshold distribution of the first photons for scenarios 3HD (in red-squares) and 3MT (in blue-circles) at 41.5 and 52.5-V Vbias, respectively.

established reference Vbias values of 41.5 V for HD and 52.5 V for MTs for subsequent tests, respectively. The correspondent CTR for these Vbias are 88 and 71 ps, respectively. MTs exhibit better stability in the region where optimal CTRs are achieved compared to the HDs. Indeed, for MTs, there is a variation of less than 4-ps across an over-voltage range larger than 5 V, while the HDs do not achieve this even within a 1-V over-voltage range. A scan of the best VthCTR is also displayed with triangle markers and dotted lines. Excluding the highest Vbias for both cases, the average VthCTR was 3 mV for the HDs and 6.5 mV for the MTs.

The same procedure was applied to scenarios 3HD* and 3MT*, yielding CTR values of 118 ps for the HDs and 79 ps for the MTs. In Scenario 3MT, a staircase plot was determined, revealing a cross-talk probability ranging between 3% and 10%. However, in Scenario 3HD, significant cross-talk contamination at very low VthCTR hides any discernible features. It is worth noting that for the older HDs, obtaining a DCR staircase plot may be unfeasible due to very high-cross-talk levels compared to the MTs, especially at low-Vbias settings [43]. In contrast, the new MTs offered a relatively straightforward process for extracting the plot from the timing channel (Fig. 8) [43].

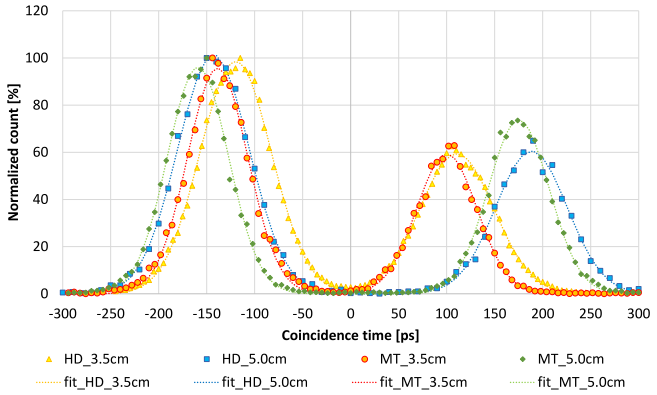

Fig. 9. DSRP coincidence time distributions for scenarios 3HD and 3MT and for both 3.5 and 5-cm distances. A double Gaussian profile is displayed for each of the four cases, including its fitting function.

TABLE IV
DSRP COMPARATIVE RESULTS

Scenarios & Distance	CTR Left	CTR Right	Gaussian Peak Distance	Equivalent Distance
3HD - 3.5 mm	88 ps	91 ps	233 ps	3.5 cm
3MT - 3.5 mm	73 ps	72 ps	237 ps	3.6 cm
3HD - 5.0 mm	89 ps	89 ps	331 ps	4.9 cm
3MT - 5.0 mm	71 ps	74 ps	334 ps	5.0 cm

C. Linearity Analysis

Regarding the linearity tests using the DSRP, the resulting distributions are plotted in Fig. 9. The area under the Gaussian distribution of the "red source" exhibits approximately 60-65% lower counts than the "white source," as was expected by their relative activities.

To calculate the spatial distancing, we employed the formula

$$\Delta x = c\frac{\Delta t}{2} \tag{1}$$

with c representing the speed of light in a vacuum, Δt denoting the time difference between the two CTR distribution fitting peaks, and Δx indicating the correlated spatial distance [14], [17]. These tests confirm the precision of NUV SiPMs from FBK. As shown in table IV, CTR values align with what was previously calculated, and the linearity is confirmed with an error lower than 2 mm. We have estimated the overall uncertainty to be approximately ± 1.7 mm, considering the oscilloscope resolution, alignment precision, and Gaussian fit uncertainties.

D. CTR Scenarios Comparison

Utilizing the previously mentioned optimum Vbias settings, we have performed tests for the remaining scenarios (1, 2, and 4). Considering the FastIC, programming the boards accurately, especially in Scenario 2, proved to be a demanding task. Here, the amplified input from the timing channel of the CM-HF led to saturation in the ASIC readings.

In the last scenario, we only conducted a VthCTR scan on both CM-HF* channels for the MT to evaluate the energy channel's timing capabilities. As expected, the timing channel

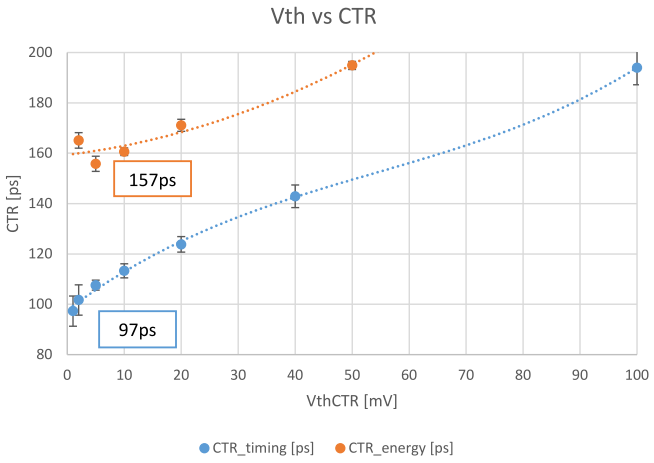

Fig. 10. Voltage threshold scan for Scenario 4MT compares energy (orange) and timing (blue) channels results using only the MT SiPMs. The dotted lines represent a polynomial fit added as an eye guide.

TABLE V
BEST CTR RESULTS

Scenario Number	Involved Tools	HD [ps]	MT [ps]
1	FastIC + RTP	129	118
2	CM-HF + FastIC + RTP	142	127
3	CM-HF + RTP	88	71
3*	CM-HF* + RTP	118	79
4*	CM-HF* + Felix	139	97

demonstrated superior performance compared to the energy one, achieving CTR values of 40 to 60-ps better, as illustrated in Fig. 10. Notably, at very low thresholds, noise dominates, posing significant challenges for data extraction and resulting in time-consuming analysis.

In Scenario 4HD*, the timing channel exhibited approximately 40-ps worse performance than 4MT*, consistent with the observations in Scenario 3*. In conclusion, the best-CTR results focusing on the timing capabilities of each acquisition chain and for both HD and MT SiPM types are summarized in Table V.

Unlike the first three, the last two scenarios have no amplification on the timing channel. Except for results with the FastIC, the presence of the amplification is relevant when using the HDs. Instead, this difference is less evident when considering the MT results.

IV. DISCUSSION

Simulations of the CM-HF confirm that the targeted frequency ranges are successfully met. In particular, the Bias-T and the timing channel effectively operate as a band-pass filter, ensuring functionality within the 10-MHz to 8-GHz frequency range. Simulation of all stages of circuit development, from schematic structuring to track dimensions and PCB layering, is necessary for applications at the target frequency range and significantly affects the outcome.

MT SiPMs have significantly shown improvement in the overall timing performance. Using MT SiPM might make dedicated high-end and high-consumption electronics unnecessary to enhance signal extraction and quality. If signals are already sufficiently strong through adequate inherent gain from the SiPM, additional high-frequency amplification may become redundant. Thus, optimizing SiPM performance is proving to be a crucial avenue for further advancements in this field, especially in the case of system-level development through multichannel architectures. Further exploration of the performance limits of MT SiPMs, particularly their operation at high or variable temperatures, will be conducted within a climate chamber.

In Fig. 7, the constant optimal threshold observed across varying bias voltages primarily reflects the system's sensitivity to initial photon detection amidst background noise. Lower thresholds may not reveal the first photon due to its proximity to noise levels. Hence, higher-thresholds effectively emerge as the signal moves away from the noise, allowing clearer detection of initial photons. This could explain the fluctuating threshold values, which seem constant but represent the point at which the first photon distinguishes itself from noise. Further detailed voltage scans could provide additional insights into this behavior.

We obtained sub-100-ps results using a combination of a fully passive readout and a commercially available system (Scenario 4MT*). Improvements in software could enhance the CTR precision in scenarios characterized by very low thresholds through in-built noise rejection algorithms to avoid detector dead time and extensive data filtering.

Data acquisition systems tailored for SiPM, especially those focused on timing, constitute an active area of research in our field. Our group focuses on developing a dedicated multichannel readout to be coupled with metascintillator structures, in particular, the so-called semi-monolithic metascintillator architecture [44]. Current ASICs, such as the PETsys TOFPET2, having an intrinsic timing resolution of around 25-ps RMS, can hardly provide the required timing precision to read out such architectures, where fast subsets are expected to have a CTR of around 70 ps. For this reason, we are investigating other integrated multichannel readout and DAQ systems. This study is the first step in developing an entirely passive multichannel readout with Balun transformers. This will be coupled to either a specific ASIC or an FPGA-based system with multiple triggering features like double ToT. Additionally, recent works [45] are addressing the potential for integrating multiple Balun transformers into a compact module considering the real-world application in PET systems.

Introducing a straightforward approach to assess system linearity through a single LOR was a side development in our studies. However, we believe a double-source phantom can provide significant insights into new detector research, especially for non-Gaussian or multispectral timing kernels. Relative activity between the sources does not need to be standardized but has to be considered when this approach is followed. The versatility of the DSRP in different scenarios can improve linearity analysis in terms of fidelity of the results.

The Felix system, based on FPGA, and paired with a passive balun-based front-end, has shown promising results in our tests. It is important to notice that FPGA technology,

while not inherently superior, offers some advantages like programmability. However, achieving scalability with FPGA-based systems is not straightforward, and presently, it might be challenging. This underscores the need for ongoing research and development to maximize these technologies' capabilities [46], [47], particularly for timing applications.

Additionally, a test combining FastIC and Felix systems was meant to be done but discarded after observing the results obtained from Scenario 1.

V. Conclusion

The integration of MT SiPMs represents a significant advancement, offering improved CTR performance (10 to 40 ps) compared to HDs due to better-cross-talk rejection and higher gain. This achievement also raises the possibility of entirely passive readout systems, potentially reducing power consumption in detector applications. Indeed, the comparison between scenarios 3 and 3* demonstrates an improvement of approximately 30 ps with the older HD SiPMs and slightly less than 10 ps with the new MTs. In particular, an interesting observation on scenarios 3HD and 3MT* can be made where an entirely passive board can match its amplified version merely by changing the SiPM. Additionally, Scenario 3MT indicates that, with the new MTs, electronics may be reaching the limit of their ability to enhance signal extraction and CTR improvement, as seen in the plateau region in Fig. 7.

Even without amplification, Felix's sub-100-ps timing capabilities demonstrate its potential for precise timing measurements. However, addressing the challenge of low statistics at very low thresholds is essential. Achieving an optimal 97 ps with a scalable solution would make FPGA-based devices compete with ASIC-based systems. Indeed, this value is only 26-ps worse than the best-possible scenario (3MT) and 21-ps better than those we obtained with the FastIC. While this ASIC shows notable capabilities, the tested functionalities have limited our results.

Acknowledgment

Special thanks to Andrea Costa, Nicola Lusardi, Fabio Garzetti, and Enrico Ronconi from Tediel S.r.l. for providing the Felix product and the technical support and help. The authors thank Francis Loignon-Houle for help with the measurements of dark counts. The research is pursued through a public–private partnership between multiwave metacrystal SA, 34 Route de la Galaise, 1228, Geneva, Switzerland, and the Instituto de Instrumentación para Imagen Molecular (I3M), Centro Mixto CSIC-UPV, Valencia, Spain. Their support is greatly acknowledged. All authors declare that they have no known conflicts of interest in terms of competing for financial interests or personal relationships that could have an influence or are relevant to the work reported in this article.

References

[1] V. Nadig, K. Herrmann, F. M. Mottaghy, and V. Schulz, "Hybrid total-body PET scanners current status and future perspectives," *Eur. J. Nucl. Med. Mol. Imag.*, vol. 49, no. 2, pp. 445–459, 2022.

[2] D. R. Schaart, "Physics and technology of time-of-flight PET detectors," *Phys. Med. Biol.*, vol. 66, no. 9, 2021, Art. no. 09TR01.

[3] K. Mikhail et al., "Development of scintillation materials for PET scanners," *Nucl. Instrum. Methods Phys. Res. A.*, vol. 571, no. 1–2, pp. 122–125, 2007.

[4] P. Lecoq, "Development of new scintillators for medical applications," *Nucl. Instrum. Methods Phys. Res. A.*, vol. 809, pp. 130–139, Feb. 2016.

[5] A. Gonzalez-Montoro et al., "Evolution of PET detectors and event positioning algorithms using monolithic scintillation crystals," *IEEE Trans. Radiat. Plasma Med. Sci.*, vol. 5, no. 3, pp. 282–305, May 2021.

[6] S. Gundacker, E. Auffray, K. Pauwels, and P. Lecoq, "Measurement of intrinsic rise times for various L(Y)SO and LuAG scintillators with a general study of prompt photons to achieve 10 ps in ToF-PET," *Phys. Med. Biol.*, vol. 61, pp. 2802–2837, Apr. 2016.

[7] V. Nadig et al., "Timing advances of commercial divalent-ion co-doped LYSO:Ce and SiPMs in sub-100 ps time-of-flight positron emission tomography," *Phys. Med. Biol.*, vol. 68, no. 7, 2023, Art. no. 75002.

[8] A. D. Guerra et al., "Advantages and pitfalls of the silicon photomultiplier (SiPM) as photodetector for the next generation of PET scanners," *Nucl. Instrum. Methods Phys. Res. A.*, vol. 617, pp. 223–226, May 2010.

[9] S. Gundacker and A. H. Heering, "The silicon photomultiplier: Fundamentals and applications of a modern solid-state photon detector," *Phys. Med. Biol.*, vol. 65, no. 17, 2020, Art. no. 17TR01.

[10] V. C. Spanoudaki and C. S. Levin, "Photo-detectors for time of flight positron emission tomography (ToF-PET)," *Sensors*, vol. 10, pp. 10484–10505, Nov. 2010.

[11] P. Lecoq and S. Gundacker, "SiPM applications in positron emission tomography: Toward ultimate PET time-of-flight resolution," *Eur. Phys. J. Plus*, vol. 136, no. 3, p. 292, 2021.

[12] N. Kratochwil, S. Gundacker, and E. Auffray, "A roadmap for sole cherenkov radiators with SiPMs in ToF-PET," *Phys. Med. Biol.*, vol. 66, no. 19, 2021, Art. no. 195001.

[13] A. Gola et al., "NUV-sensitive silicon photomultiplier technologies developed at Fondazione Bruno Kessler," *Sensors*, vol. 19, no. 2, p. 308, 2019.

[14] G. Konstantinou, P. Lecoq, J. M. Benlloch, and A. J. Gonzalez, "Metascintillators for ultrafast gamma detectors: A review of current state and future perspectives," *IEEE Trans. Radiat. Plasma Med. Sci.*, vol. 6, no. 1, pp. 5–15, Jan. 2022.

[15] G. Konstantinou et al., "A proof-of-concept of cross-luminescent metascintillators: Testing results on a BGO: BaF2 metapixel," *Phys. Med. Biol.*, vol. 68, no. 2, 2023, Art. no. 025018.

[16] F. Pagano, N. Kratochwil, M. Salomoni, M. Pizzichemi, M. Paganoni, and E. Auffray, "Advances in heterostructured scintillators: Toward a new generation of detectors for ToF-PET," *Phys. Med. Biol.*, vol. 67, no. 13, 2022, Art. no. 135010.

[17] P. Lecoq, "On the way to the 10 ps time-of-flight PET challenge," *Eur. Phys. J. Plus*, vol. 137, no. 8, pp. 1–7, 2022.

[18] S. Kwon et al., "Ultrafast timing enables reconstruction-free positron emission imaging," *Nat. Photon.*, vol. 15, no. 12, pp. 914–918, 2021.

[19] H. T. Leem, Y. Choi, J. Jung, K. Park, Y. K. Kim, and J. H. Jung, "Optimized ToF-PET detector using scintillation crystal array for brain imaging," *Nucl. Eng. Technol.*, vol. 54, no. 7, pp. 2592–2598, 2022.

[20] S. Gundacker et al., "Experimental time resolution limits of modern SiPMs and ToF-PET detectors exploring different scintillators and cherenkov emission," *Phys. Med. Biol.*, vol. 65, no. 2, 2020, Art. no. 025001.

[21] S. Merzi et al., "NUV-HD SiPMs with metal-filled trenches," *J. Instrum.*, vol. 18, no. 5, 2023, Art. no. P05040.

[22] R. Latella, A. J. Gonzalez, J. M. Benlloch, P. Lecoq, and G. Konstantinou, "Minimizing power consumption for time-of-flight PET SiPM readout," in *Proc. IEEE Nucl. Sci. Symp. Med. Imag. Conf. (NSS/MIC)*, 2022, pp. 1–3.

[23] S. Gómez et al., "FastIC: A highly configurable ASIC for fast timing applications," in *Proc. IEEE Nucl. Sci. Symp. Med. Imag. Conf. (NSS/MIC)*, 2021, pp. 1–4.

[24] N. Corna, F. Garzetti, N. Lusardi, and A. Geraci, "Digital instrument for time measurements: Small, portable, high–performance, fully programmable," *IEEE Access*, vol. 9, pp. 123964–123976, 2021.

[25] N. Lusardi, N. Corna, F. Garzetti, S. Salgaro, and A. Geraci, "Cross-talk issues in time measurements," *IEEE Access*, vol. 9, pp. 129303–129318, 2021.

[26] E. Ronconi, N. Corna, A. Costa, F. Garzetti, N. Lusardi, and A. Geraci, "Multi-COBS: A novel algorithm for byte stuffing at high throughput," *IEEE Access*, vol. 10, pp. 78848–78859, 2022.

[27] A. Costa, N. Corna, F. Garzetti, N. Lusardi, E. Ronconi, and A. Geraci, "High-performance computing of real-time and multichannel histograms: A full FPGA approach," *IEEE Access*, vol. 10, pp. 47524–47540, 2022.

[28] S. Gundacker, R. M. Turtos, E. Auffray, M. Paganoni, and P. Lecoq, "High-frequency SiPM readout advances measured coincidence time resolution limits in ToF-PET," *Phys. Med. Biol.*, vol. 64, no. 5, 2019, Art. no. 055012.

[29] R. Latella, A. J. Gonzalez, J. Barrio, J. M. Benlloch, P. Lecoq, and G. Konstantinou, "Test setup and data selection protocols for the measurement of metascintillator CTR," in *Proc. IEEE Nucl. Sci. Symp. Med. Imag. Conf. (NSS/MIC)*, 2021, pp. 1–4.

[30] R. Latella et al., "Exploiting cherenkov radiation with BGO-based metascintillators," *IEEE Trans. Radiat. Plasma Med. Sci.*, vol. 7, no. 8, pp. 810–818, Nov. 2023.

[31] L. Sun, Y. Chen, K. Sun, and W. Wu, "Analysis of differential balun circuits," in *Proc. Int. Symp. Signals, Syst. Electron.*, 2010, pp. 1–4.

[32] J. W. Cates and C. S. Levin, "Evaluation of a clinical ToF-PET detector design that achieves $\leq$100 ps coincidence time resolution," *Phys. Med. Biol.*, vol. 63, no. 11, 2018, Art. no. 115011.

[33] R. Reeder, *How to Design Wideband Front Ends for GSPs Converters*. Analog Devices, Wilmington, MA, USA, 2013.

[34] K.-Y. Jang, H.-S. Oh, H.-C. Jeong, and K.-W. Yeom, "Design of a planar wideband microwave bias-tee using lumped elements," *J. Korean Inst. Electromagn. Eng. Sci.*, vol. 24, no. 4, pp. 384–393, 2013.

[35] H.-S. Oh, H.-C. Jeong, and K.-W. Yeom, "Design of a microwave bias-tee using lumped elements with a wideband characteristic for a high power amplifier," *J. Korean Inst. Electromagn. Eng. Sci.*, vol. 22, pp. 683–693, Jul. 2011.

[36] J. Glaser, "Optimizing performance of a pulsed laser diode driver based on a GaN FET," in *Proc. IEEE Workshop Wide Bandgap Power Devices Appl. Asia*, 2019, pp. 1–5.

[37] G. Chen, C. Wiede, and R. Kokozinski, "Data processing approaches on spad-based d-ToF LiDAR systems: A review," *IEEE Sens. J.*, vol. 21, no. 5, pp. 5656–5667, Mar. 2021.

[38] X. Qian, W. Jiang, A. Y. Elsharabasy, and M. J. Deen, "Modeling for single-photon avalanche diodes: State-of-the-art and research challenges," *Sensors*, vol. 23, no. 7, p. 3412, 2023.

[39] A. Gola, A. Ferri, A. Tarolli, N. Zorzi, and C. Piemonte, "SiPM optical crosstalk amplification due to scintillator crystal: Effects on timing performance," *Phys. Med. Biol.*, vol. 59, no. 13, pp. 3615–3635, 2014.

[40] N. Kratochwil, E. Auffray, and S. Gundacker, "Exploring cherenkov emission of BGO for TOF-PET," *IEEE Trans. Radiat. Plasma Med. Sci.*, vol. 5, no. 5, pp. 619–629, Sep. 2021.

[41] E. Lamprou, A. J. Gonzalez, F. Sanchez, and J. M. Benlloch, "Exploring ToF capabilities of PET detector blocks based on large monolithic crystals and analog SiPMs," *Phys. Med.*, vol. 70, pp. 10–18, Feb. 2020.

[42] J. Nuyts, M. Defrise, S. Gundacker, E. Roncali, and P. Lecoq, "The SNR of positron emission data with gaussian and non-gaussian time-of-flight kernels, with application to prompt photon coincidence," *IEEE Trans. Med. Imag.*, vol. 42, no. 5, pp. 1254–1264, May 2023.

[43] V. Nadig et al., "A comprehensive study on the timing limits of the ToFPET2 ASIC and on approaches for improvements," *IEEE Trans. Radiat. Plasma Med. Sci.*, vol. 6, no. 8, pp. 893–903, Nov. 2022.

[44] G. Konstantinou et al., "Semi-monolithic meta-scintillator simulation proof-of-concept, combining accurate doi and ToF," *IEEE Trans. Radiat. Plasma Med. Sci.*, vol. 8, no. 5, pp. 482–492, May 2024.

[45] V. Nadig, M. Hornisch, J. Oehm, K. Herweg, V. Schulz, and S. Gundacker, "16-channel SiPM high-frequency readout with time-over-threshold discrimination for ultrafast time-of-flight applications," *EJNMMI Phys.*, vol. 10, no. 1, p. 76, 2023.

[46] J. Qin, D. Guo, L. Zhao, S. Lan, Y. Wang, and Q. An, "Design and performance of a 16-channel coarse-fine TDC prototype ASIC," *Nucl. Instrum. Methods Phys. Res. A.*, vol. 1050, May 2023, Art. no. 168167.

[47] D. Kim, Y. Choi, and S. Lee, "An improved method of FPGA-based TDC for time-of-flight PET," in *Proc. IEEE Nucl. Sci. Symp. Med. Imag. Conf. (NSS/MIC)*, 2013, pp. 1–3.